

Matrix-Isolation FT-IR Study and Theoretical Calculations of the Hydrogen-Bond Interaction of Hypoxanthine with H₂O

Riet Ramaekers,[†] Ahmed Dkhissi,[‡] Ludwik Adamowicz,[§] and Guido Maes^{*,†}

Department of Chemistry, University of Leuven, Celestijnenlaan 200F, B-3001 Heverlee, Belgium, Laboratory of Novel materials, University of Mons, 20 Place du Parc, 7000 Mons, Belgium, and Department of Chemistry, University of Arizona, Tucson, Arizona 85721

Received: September 24, 2001; In Final Form: February 4, 2002

The H-bonding interaction between the oxopurine base *hypoxanthine* and water is investigated using matrix-isolation FT-IR spectroscopy combined with theoretical density functional theory and ab initio methods. For vibrational frequency predictions, only the DFT/B3-LYP method is used, while for the prediction of relative energies and H-bond interaction energies of the complexes, four different theoretical methods are compared, i.e., RHF//RHF, MP2//RHF, DFT//DFT, and MP2//DFT. The oxo-N1H–N7H, the oxo-N1H–N9H, and the hydroxy-N9H (rotamer with the hydroxy-H atom pointed toward the N1 atom) are found to be the three most stable tautomeric forms of the free base. Different, stable complexes between these three tautomers and water have been predicted theoretically. The experimental FT-IR spectra agree well with this prediction, and most of the characteristic spectral data for the four most stable closed complexes, N7–H···O–H···O=C6 and N1–H···O–H···O=C6 of the O17 tautomer and N1–H···O–H···O=C6 and N9–H···O–H···N3 of the O19 tautomer, have been identified in the spectrum. The closed complexes with two H-bonds are the most stable systems due to the H-bond cooperative effect. The obtained results allow to analyze the important relation between cooperativity and (non-)linearity of N–H···OH-bonded systems.

Introduction

Tautomerism and H-bonding are significant aspects in biochemical and pharmacological research. Because recognition between different molecules is a requirement for biological molecules to find their correct reactive pathways, structural differences between tautomers are of huge importance.¹

The oxopurine base hypoxanthine is of considerable interest because it is an important intermediate in the purine metabolism; i.e., the nucleotide analogue of hypoxanthine, inosinate, is the precursor of adenylate (AMP) and guanylate (GMP).² Hypoxanthine is also occasionally found in minor amounts in tRNA. Adenine in DNA can be oxidatively deaminated by nitrous acid to form hypoxanthine. Hypoxanthine in DNA is a potentially mutagenic compound, since it can code for guanine instead of adenine and form a base pair with cytosine during DNA replication, giving rise to A·T → G·C transitions.³

A former combined matrix-isolation FT-IR and theoretical study (DFT/B3-LYP) on the tautomeric properties of hypoxanthine has led to the conclusion that the oxo form O17 of this base is the most abundant tautomer, but two other forms, O19 and H9-r1, are also relatively stable and are observed experimentally in a low-temperature Ar matrix.⁴ The mean experimental values of the tautomeric equilibrium constant K_T (O17 ⇌ O19) obtained with the RHF and DFT intensities are 0.40 and 0.72, respectively. For the equilibrium O17 ⇌ H9-r1, the experimental K_T values are 0.04 and 0.03 for RHF and DFT, respectively.

The combination of theoretical methods with experimental data from matrix-isolation FT-IR spectroscopy is a suitable method for the study of the tautomeric and H-bonding properties of polyfunctional bases such as hypoxanthine. Water is an extremely suitable model molecule because it can interact simultaneously as a proton donor and as a proton acceptor. In some of our previous studies, this combined study has allowed a detailed description of the tautomeric and H-bonding behavior of pyridines (4-OH and 3-OH),⁵ pyrimidines (2-OH, 5-Br-2-OH),⁶ and some nucleic acid bases (1-CH₃-cytosine⁷ and adenine⁸). Combination of matrix-isolation FT-IR experiments with theory has a double advantage. On one hand, accurate theoretical methods are a condition-sine-qua-non for the interpretation of the highly complicated experimental spectra for H-bonded polyfunctional bases such as the nucleic acid bases. On the other hand, such a comparison also allows the different theoretical methods to be checked for their accuracy to predict tautomeric and H-bonding properties. As a continuation of this line of study,^{5–8} we present in this paper also some new interesting correlations deduced from this comparison between experiment and theory.

Methodology

Experimental Method. The studied compound (hypoxanthine, ≥99%) was purchased from Fluka. High-purity argon gas (N60 = 99.999 90%) was obtained from Air Liquide. The Ar/H₂O mixtures with different Ar/H₂O ratio were prepared in a glass vacuum line. Bidistilled water was used for the water-doped matrixes. Similar to our former studies on water complexes in Ar matrixes, the base/water ratio varied between 1:1 and 1:5. The latter ratio ensures that an excess amount of 1:1 base–H₂O complexes is present in the Ar matrix with only weak spectral manifestations of higher stoichiometry complexes.

* Corresponding author. E-mail: guido.maes@chem.kuleuven.ac.be. Fax: 016/32 79 92.

[†] University of Leuven.

[‡] University of Mons.

[§] University of Arizona.

TABLE 1: Total (au) and Relative Energies (kJ·mol⁻¹) of Different Tautomers and Rotamers of Hypoxanthine Calculated at the RHF//RHF, MP2//RHF, DFT//DFT, and MP2//DFT Levels of Theory with the 6-31++G Basis Set**

	RHF ^a // RHF 6-31++G**	ΔE^b RHF// RHF	μ , D (RHF)	MP2 ^a // RHF 6-31++G**	ΔE^b MP2// RHF	DFT ^c // DFT 6-31++G**	ΔE^b DFT// DFT	μ , D (DFT)	MP2 ^c // DFT 6-31++G**	ΔE^b MP2// DFT
O17	-484.277 499	0.00	1.46	-485.754 608	0.00	-487.121 606	0.00	1.56	-485.762 000	0.00
O19	-484.276 871	1.65	5.81	-485.753 030	4.14	-487.120 373	3.24	5.43	-485.760 817	3.11
H9-r1 ^f	-484.274 481	7.92	2.59	-485.749 887	12.39	-487.115 061	17.18	2.58	-485.756 877	13.45
H9-r2 ^g	-484.271 976	14.50	4.91	-485.747 972	17.42	-487.112 887	22.89	4.78	-485.754 905	18.63
H7-r1 ^f	-484.269 171	21.87	5.28	-485.746 468	21.37	-487.111 226	27.25	5.12	-485.753 126	23.30
O37	-484.265 120	32.50	5.36	-485.741 938	33.27	-487.109 809	30.97	5.09	-485.749 380	33.13
H3-r2 ^g	484.253 971 ^d	61.77	3.73	-485.732 909 ^d	56.97	-487.099 461 ^d	58.14	3.35	-485.740 531 ^d	56.37
H7-r2 ^g	-484.254 985	59.11	6.97	-485.732 807	57.24	-487.098 078	61.77	6.73	-485.739 448	59.21
H3-r1 ^f	-484.251 613 ^d	67.96	6.31	-485.730 372 ^d	63.63	-487.097 524 ^d	63.23	5.71	-485.738 180 ^d	62.54
H1-r2 ^g	-484.244 349 ^d	87.04	6.77	-485.723 247 ^d	82.34	-487.089 891 ^d	83.27	6.44	-485.731 245 ^d	80.75
O39	-484.243 667 ^e	88.83	11.65	-485.719 284 ^e	92.74	-487.087 856 ^e	88.61	11.23	-485.727 044 ^e	91.78

^a ZPE-corrected RHF and MP2 energies; ZPE values scaled with uniform scaling factor 0.900 (RHF). ^b Energy difference between the tautomers and rotamers. ^c ZPE corrected DFT and MP2 energies; ZPE values scaled with uniform scaling factor 0.970 (DFT). ^d ZPE contribution not calculated; ZPE value of the hydroxy-N₉H form is used. ^e ZPE contribution not calculated; ZPE value of the oxo-N₁H-N₇H form is used. ^f r1: rotamer with the hydroxy H atom pointed toward the N₁ atom. ^g r2: rotamer with the hydroxy H atom pointed toward the N₇ atom.

The cryogenic and FT-IR (Bruker IFS-88) equipments used here have been described in detail previously.^{9,10} For evaporation of the solid compound hypoxanthine into the jet of argon/H₂O, a homemade minifurnace was positioned inside the cryostat close to the CsI cold window (14 K). The optimal sublimation temperature for hypoxanthine was found to be 168 °C.

Theoretical Method. The geometries, the energies, and the vibrational frequencies of the different H-bonding complexes were calculated with the density functional theory (DFT) and with the RHF methodology. For the DFT method, the Becke three-parameter hybrid functional¹¹ combined with the Lee, Yang, and Parr correlation functional¹² was used. This method gives quite accurate results for hydrogen-bonded systems modeling the H-bonded DNA bases, as has been shown in former studies.^{13,14} In particular, the shift of the important O–H stretching frequency of the proton-donor molecule in the H-bonded complex is much better predicted with the B3-LYP functional compared to other functionals or with ab initio methods.

For the molecular orbital expansion we have used the 6-31++G** basis set. The choice of this basis set is based on the consideration that in order to obtain reliable properties for H-bonded systems, it is essential to use a basis set with sufficient diffuseness and angular flexibility.¹⁵ This basis set is sufficient to predict reliable structural and vibrational properties for H-bonded systems, as has been demonstrated earlier.^{13–14}

The optimizations of the geometries of the different complexes with the RHF and DFT methods were followed by single-point energy calculations at the MP2 level using the same basis set. These methods will be denoted as MP2//RHF and MP2//DFT, respectively. According to earlier studies, the B3-LYP/6-31++G** geometries for H-bonded complexes are much closer to the experimental geometries than the RHF/6-31++G** geometries.^{16,17} For this reason, the results obtained with the MP2//DFT method are more reliable than those obtained with the MP2//RHF method. Nevertheless, the RHF calculations are still performed for the sake of comparison with previous work on similar systems and to complete earlier established correlations between different H-bond parameters.^{18,19}

The total energy for each complex includes the zero-point vibrational energy correction. This ZPE value is scaled with a constant scaling factor of 0.900 for the RHF method and with 0.970 for the DFT method. The interaction energies are calculated as the difference between the total energy of the complex and the sum of the energies of the separate subunits, i.e., the monomer base and water. The Boys–Bernardi counterpoise correction²⁰ is additionally applied to obtain the basis-

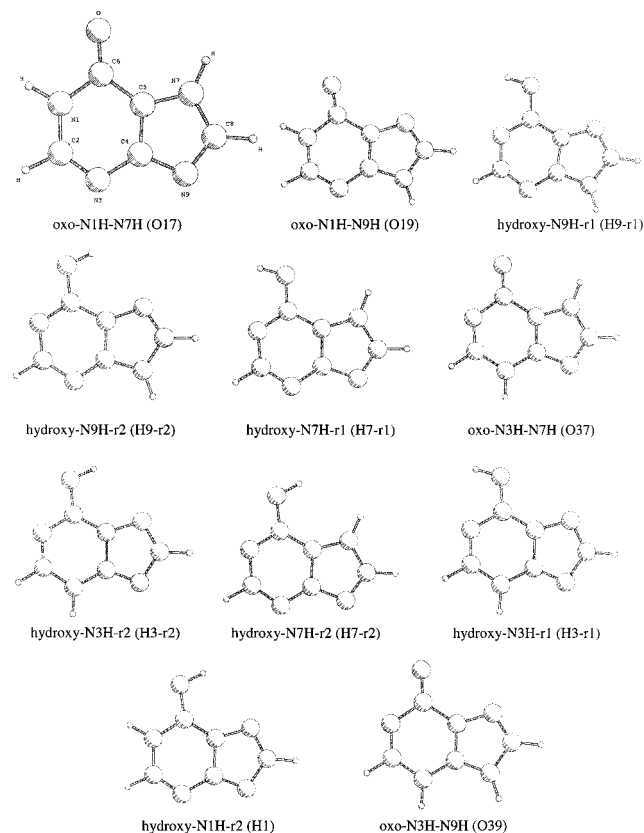
set-superposition-error (BSSE) corrected interaction energies. The IR frequencies and intensities are computed by using analytical derivative procedures implemented in the Gaussian 94 and Gaussian 98 programs.^{21,22}

Finally, potential energy distributions (PED) are calculated and the predicted IR frequencies are scaled to account for various systematic errors in the theoretical approach, i.e., the use of a finite basis set, the neglect of vibrational anharmonicity, and the incomplete account for electron correlation effects. Two scaling procedures are applied. Either all frequencies are scaled with a uniform scaling factor of 0.900 for RHF and 0.970 for DFT,^{13,14} or scaling is performed with a set of different scaling factors depending on the different types of vibrational modes, i.e., 0.950 for $\nu(\text{XH})$, 0.980 for the out-of-plane modes, and 0.975 for all other modes. The latter procedure is only used for the DFT method. These optimal scaling factors are computed by using the ratio of experimental to computed frequencies. The use of different scaling factors for vibrational frequencies has been proposed by several authors in the past.^{23–26}

Results and Discussion

Monomeric Hypoxanthine.⁴ The total energies (ZPE corrected), the relative energies, and the dipole moments of the different tautomeric forms of hypoxanthine are presented in Table 1. Eight stable tautomers are found for hypoxanthine (Chart 1): four oxo forms (denoted as O17, O19, O37, and O39) and four hydroxy forms (denoted as H9, H7, H3, and H1). For all the hydroxy forms except H1, two rotamers exist (denoted as r1 and r2), depending on the orientation of the OH group. It must be mentioned that two other forms, H1-r1 and O13, predicted by Costas et al.,²⁷ have not been found in our calculations. According to all theoretical methods, the oxo form O17 is the most stable one, followed by the O19 form. Prototropy in the five-ring causes only a small energy difference (about 3 kJ·mol⁻¹ (MP2//DFT)). In the six-ring, the N1H arrangement is preferred over the N3H arrangement in the oxo tautomers. For the hydroxy forms, the H9-r1 tautomer is the most stable one. The larger relative energy difference between the H7 rotamers than between the H3 and H9 rotamers can be explained by the repulsion between the H atoms on the O and the N7 atoms, which leads to a stability decrease of the H7-r2 form.

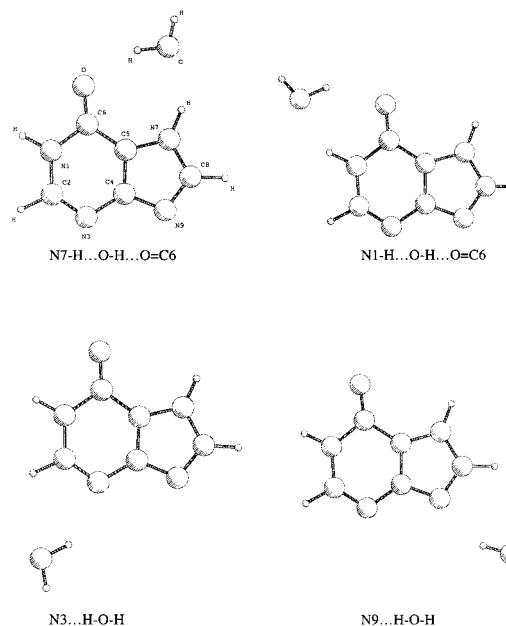
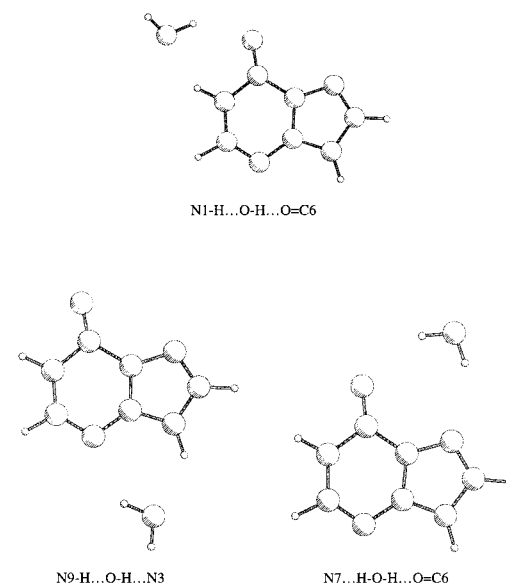
The most stable form, O17, has the smallest calculated dipole moment compared to all other forms. One might therefore expect a shift in the stability order in more polar environments, similar to what has been found for 2-hydroxypyri(mi)dine/2-oxopyri(mi)dine.^{6,17,28}

CHART 1: Geometries of Hypoxanthine Tautomers and Rotamers

A good agreement between the complicated experimental spectrum and the, formerly, low-resolution spectrum by Sheina et al.²⁹ is found. In a former paper,⁴ the complete spectral analysis for monomer hypoxanthine has allowed us to identify three different tautomers in the spectrum, i.e., the O17, the O19, and the H9-r1 forms. A mean frequency deviation of 27.1 cm^{-1} between experimental and calculated frequencies is obtained for the RHF method, which decreases to 15.1 cm^{-1} for the DFT method with a single scaling factor. The use of variable scaling factors improves this value down to 9.8 cm^{-1} for the DFT method.

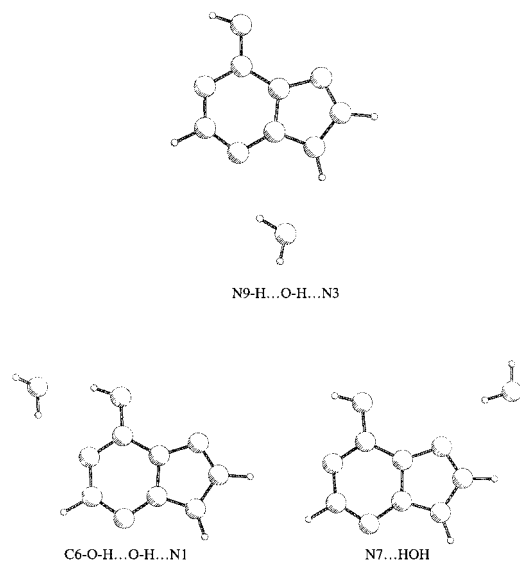
Combination of experimental and theoretical intensities of some characteristic bands of the O19 or H9-r1 form with some bands of the O17 form has allowed estimation of the position of the tautomeric equilibria $\text{O17} \rightleftharpoons \text{O19}$ and $\text{O17} \rightleftharpoons \text{H9-r1}$. A K_T value of 0.40 (RHF) or 0.72 (DFT) has been found for $\text{O17} \rightleftharpoons \text{O19}$, whereas the theoretically predicted ($\Delta E_T(\text{OK}) \approx \Delta G_T^\circ(T) = \Delta H_T^\circ - T\Delta S_T^\circ = -RT \ln K_T$) value was 0.32, 0.43, 0.41, and 0.64, obtained with MP2//RHF, MP2//DFT, DFT//DFT, and RHF//RHF, respectively. For the second equilibrium $\text{H9-r1} \rightleftharpoons \text{O17}$, the experimental values are 0.04 and 0.03 for RHF and DFT, respectively, whereas the predicted values are 0.03, 0.02, 0.01, and 0.11 for MP2//RHF, MP2//DFT, DFT//DFT, and RHF//RHF, respectively.

H-Bonded Complexes Hypoxanthine·H₂O. This study is limited to the investigation of the H-bond interaction between the three most stable hypoxanthine tautomers O17, O19, and H9-r1, which are experimentally detected in an Ar matrix and water. These three forms have several different H-bonding sites, i.e., N···, N-H···, C=O···, and C-O-H···. Charts 2–4 illustrate the predicted stable H-bonded geometries of complexes of hypoxanthine with a single water molecule. We have obtained four stable H-bonded complexes for the O17 tautomer and three

CHART 2: Geometries of the H-Bonded Complexes between (O17) Hypoxanthine and Water**CHART 3: Geometries of the H-Bonded Complexes between (O19) Hypoxanthine and Water**

stable complexes for the O19 and the H9-r1 forms. The total and relative energies and the dipole moments of all these complexes are summarized in Table 2, whereas the interaction energies are listed in Table 3.

The $\text{N7-H}\cdots\text{O-H}\cdots\text{O=C6}$ structure is the most stable structure among the four isomeric complexes of the O17 tautomer. This is a so-called “closed complex”, because it is stabilized by two nonlinear H-bonds, $\text{N7-H}\cdots\text{O}$ (H-bond angle: 146°) and $\text{O-H}\cdots\text{O=C6}$ (158°). The $\text{N1-H}\cdots\text{O-H}\cdots\text{O=C6}$ complex of the O17 tautomer is $10.51 \text{ kJ}\cdot\text{mol}^{-1}$ (MP2//DFT) less stable than the first complex. Although two similar H-bonds stabilize this structure, they are more nonlinear than in the first complex, i.e., $\text{N1-H}\cdots\text{O}$ (143°) and $\text{O-H}\cdots\text{O=C6}$ (146°), which might explain the rather large difference in stability. The larger acidity of the N7-H group, which is easily understood from the resonance structures, is another suggestion for the difference in stability between the two

CHART 4: Geometries of the H-Bonded Complexes between (H9-r1) Hypoxanthine and Water


complexes. The two other complexes of the O17 tautomer are open complexes, stabilized by a single H-bond, i.e., $N3\cdots H-O$ (152°) and $N9\cdots H-O$ (164°) for the $N3\cdots H-OH$ and the $N9\cdots H-OH$ complexes, respectively. H-bond cooperativity³⁰ between the two H-bonds in the closed complexes is clearly manifested by the differences in interaction energies between the closed and the open complexes (Table 3). Similar results have been obtained in former works of our group.^{6,17,31,32}

For the tautomer O19, all three isomeric complexes are closed and stabilized by two nonlinear H-bonds. The stability order of the first two complexes ($N1-H\cdots O-H\cdots O=C6$ and $N9-H\cdots O-H\cdots N3$) can be explained in the same way as for the closed complexes of the O17 tautomer; i.e., the greater linearity of the H-bonds reflects a greater strength of the H-bonds. The third complex $N7\cdots H-O-H\cdots O=C6$ is an example of a closed H-bonded complex characterized by "anticooperativity", implying that two H-bonds of the same kind weaken each other.³⁰ This complex is less stable, although it is also closed by two H-bonds, because the two "acidic" O-H sites of water simultaneously act as a proton donor. The interaction energy of this closed complex is only slightly larger than the interaction energy of an open complex (Table 3).

For the H9-r1 tautomer, two closed complexes, $C6-O-H\cdots O-H\cdots N1$ and $N9-H\cdots O-H\cdots N3$, and one open complex, $N7\cdots H-OH$, are predicted. All these complexes are at least $22.6 \text{ kJ}\cdot\text{mol}^{-1}$ (MP2//DFT) (Table 2) less stable than the most stable $N7-H\cdots O-H\cdots O=C6$ complex of the O17 tautomer.

As can be noted from Tables 2 and 3, all theoretical methods predict the same stability order for all the complexes. The $N7-H\cdots O-H\cdots O=C6$ complex of the O17 tautomer is the most stable structure with the largest interaction energy value. The second most stable form is the $N1-H\cdots O-H\cdots O=C6$ complex, also from the O17 tautomer. This means that the complexation of hypoxanthine with one water molecule induces no tautomeric shift in the stability order of the free tautomers O17, O19, and H9-r1. This result is in conflict with what was expected from the calculated dipole moments; i.e., the O17 form has the smallest calculated dipole moment compared to all other forms. A tautomeric shift has been observed earlier for other nucleic acid bases and model molecules, such as 2-hydroxypyridine/2-oxopyridine.^{6,17,28} At first sight, this result is also in conflict with the recently published results of Shukla et al.,³³ since these

authors have found that hydration slightly favors the O19 form over the O17 form. However, only a single H-bond interaction site of hypoxanthine has been considered in the latter work.

Spectral Properties. The different regions of the FT-IR spectra of hypoxanthine/ H_2O /Ar are shown in Figures 1–3. The experimental and theoretical vibrational analysis for the most perturbed (H-bond affected) vibrational modes of the four most stable complexes are summarized in Tables 4–7.

From the theoretically predicted frequency shifts for the H-bonding sensitive modes ν_{N-H} , $\nu_{C=O}$, δ_{N-H} , γ_{N-H} , and $\gamma_{C=O}$ of the base and the free and bonded water modes ν_{O-H}^f and ν_{O-H}^b (Tables 4–7), the $\nu_{C=O}$ spectral region is expected to be the most suitable region for discrimination among the four different H-bonded complexes $N7-H\cdots O-H\cdots O=C6$ and $N1-H\cdots O-H\cdots O=C6$ of O17 and $N1-H\cdots O-H\cdots O=C6$ and $N9-H\cdots O-H\cdots N3$ of O19. We will therefore first analyze the spectral region $1800\text{--}1400 \text{ cm}^{-1}$, which also contains the shifted δ_{N-H} mode and the bending mode $\delta_{(H_2O)}$.

$\nu_{C=O}$, δ_{H_2O} , and δ_{N-H} Region ($1800\text{--}1400 \text{ cm}^{-1}$) (Figure 1). Addition of water to hypoxanthine/Ar matrixes affects the $\nu_{C=O}$ spectral region considerably. As a matter of fact, the relative intensities of the quadruplet $1753/1742/1734/1728 \text{ cm}^{-1}$ $\nu_{C=O}$ absorption of the free oxo tautomers O17 and O19 clearly change, and new, broader bands grow in at 1722 and $\pm 1700 \text{ cm}^{-1}$ (Figure 1). Since the $\nu_{C=O}$ components $1734/1728 \text{ cm}^{-1}$ have been assigned to the O17 tautomer⁴ and the new band at $\pm 1700 \text{ cm}^{-1}$ is shifted $-34/-28 \text{ cm}^{-1}$ from these free absorptions, this band can be assigned to the $\nu_{C=O}$ absorption in the $N7-H\cdots O-H\cdots O=C6$ complex of the O17 tautomer, the predicted shift being -33 cm^{-1} (Table 4). The other new band observed at 1722 cm^{-1} is shifted $-31/-20 \text{ cm}^{-1}$ from the free O19 $\nu_{C=O}$ absorption components $1753/1742 \text{ cm}^{-1}$, and comparison with the predicted shift (-27 cm^{-1} , Table 6) for the $N1-H\cdots O-H\cdots O=C6$ complex of the O19 tautomer allows assignment of this band to the $\nu_{C=O}$ mode in the latter complex. The larger experimental intensity of the complex $\nu_{C=O}$ band at 1700 cm^{-1} compared to that at 1722 cm^{-1} is consistent with the larger predicted stability of the $N7-H\cdots O-H\cdots O=C6$ complex of O17 compared to that of $N1-H\cdots O-H\cdots O=C6$ of O19, since the predicted complex intensities are not very different (758 versus $717 \text{ km}\cdot\text{mol}^{-1}$). This is also clearly reflected by the larger intensity decrease of the free $\nu_{C=O}$ components $1734/1728 \text{ cm}^{-1}$ (O17) compared to $1753/1742 \text{ cm}^{-1}$ (O19).

The alternative complex $N1-H\cdots O-H\cdots O=C6$ of O17 is characterized by a predicted shift $\Delta\nu_{C=O}$ of -19 cm^{-1} (Table 5). A weak, new shoulder at 1715 cm^{-1} is observed in water-doped matrixes, and the shift of $-19/-13 \text{ cm}^{-1}$ is consistent with the predicted shift for the $N1-H\cdots O-H\cdots O=C6$ complex of O17. Estimation of the relative intensity compared to the earlier assigned complex bands at 1722 and 1700 cm^{-1} is not possible, because the bands at 1722 and 1715 cm^{-1} are too close and 1715 cm^{-1} has a very small intensity.

For the fourth complex, $N9-H\cdots O-H\cdots N3$, of the O19 tautomer, a positive shift of $+4 \text{ cm}^{-1}$ is predicted for the $\nu_{C=O}$ mode, which is not involved in the H-bonding in this case. Maybe the very weak and sharper new splittings observed at 1757 cm^{-1} ($+4 \text{ cm}^{-1}$) and 1749 cm^{-1} ($+7 \text{ cm}^{-1}$) at larger H_2O concentrations in the matrixes could be due to the presence of a small amount of the $N9-H\cdots O-H\cdots N3$ complex of O19 hypoxanthine, but this assignment is only tentative.

The observed and predicted $\Delta\nu_{C=O}$ shifts are, at least semiquantitatively, consistent with the $\Delta r_{C=O}$ distance changes (Table 8) in the four complexes considered here. As a matter

TABLE 2: Total (au) and Relative Energies (kJ·mol⁻¹) of H-Bonded Complexes of Different Tautomers of Hypoxanthine with Water

	RHF ^a //RHF 6-31++G**	ΔE^b RHF// RHF	μ, D (RHF)	MP2 ^a //RHF 6-31++G**	ΔE^b MP2// RHF	DFT ^c //DFT 6-31++G**	ΔE^b DFT// DFT	μ, D (DFT)	MP2 ^c //DFT 6-31++G**	ΔE^b MP2// DFT
O17 tautomer										
N7H···OH···O=C6	-560.302 364	0.0	3.19	-561.985 760	0.0	-563.552 770	0.0	3.03	-561.994 298	0.0
N1H···OH···O=C6	-560.299 673	7.06	3.26	-561.981 960	9.98	-563.549 114	9.60	3.12	-561.990 294	10.51
N3···HOH	-560.295 301	18.54	2.01	-561.976 503	24.30	-563.543 693	23.83	3.59	-561.984 825	24.87
N9···HOH	-560.295 399	18.29	2.44	-561.976 500	24.31	-563.543 506	24.32	2.98	-561.984 736	25.10
O19 tautomer										
N1H···OH···O=C6	-560.299 780	6.78	4.08	-561.981 011	12.47	-563.548 544	11.10	4.21	-561.989 678	12.13
N9H···OH···N3	-560.297 130	13.74	7.27	-561.979 702	15.91	-563.546 240	17.14	6.38	-561.988 701	14.69
N7···HOH···O=C6	-560.296 082	16.49	8.92	-561.976 433	24.49	-563.543 334	24.77	8.71	-561.985 045	24.29
H9-r1 tautomer										
N9H···OH···N3	-560.295 834	17.14	3.24	-561.977 474	21.75	-563.542 119	27.96	2.79	-561.985 688	22.61
C6OH···OH···N1	-560.294 555	20.50	3.30	-561.976 055	25.48	-563.542 043	28.16	3.42	-561.984 181	26.56
N7···HOH	-560.292 045	27.09	1.70	-561.971 772	36.73	-563.536 932	41.58	2.86	-561.979 585	38.63

^a ZPE-corrected RHF and MP2 energies; ZPE values scaled with uniform scaling factor 0.900 (RHF). ^b Energy difference between the complexes, relative to the N7–H···O–H···O=C6 complex of the O17 tautomer. ^c ZPE-corrected DFT and MP2 energies; ZPE values scaled with uniform scaling factor 0.970 (DFT).

TABLE 3: H-Bond Interaction Energies (kJ·mol⁻¹) of Hypoxanthine–Water H-Bonded Complexes

	RHF//RHF	MP2//RHF	DFT//DFT	MP2//DFT
Tautomer 1: Oxo-N1HN7H (O17)				
N7H···OH···O=C6				
ΔE	-46.41	-59.68	-56.39	-61.36
$\Delta E + \Delta ZPE$	-37.69	-50.96	-46.42	-51.39
$\Delta E + \Delta ZPE$ -BSSE	-34.36	-41.56	-42.23	-39.32
N1H···OH···O=C6				
ΔE	-38.39	-48.75	-45.98	-50.03
$\Delta E + \Delta ZPE$	-30.62	-40.98	-36.82	-40.87
$\Delta E + \Delta ZPE$ -BSSE	-28.04	-33.39	-33.30	-30.94
N3···HOH				
ΔE	-25.29	-32.80	-29.35	-33.27
$\Delta E + \Delta ZPE$	-19.14	-26.65	-22.59	-26.52
$\Delta E + \Delta ZPE$ -BSSE	-17.22	-21.16	-20.40	-19.92
N9···HOH				
ΔE	-25.45	-32.69	-28.82	-33.01
$\Delta E + \Delta ZPE$	-19.40	-26.64	-22.10	-26.28
$\Delta E + \Delta ZPE$ -BSSE	-17.35	-21.10	-19.61	-19.46
Tautomer 2: Oxo-N1HN9H (O19)				
N1H···OH···O=C6				
ΔE	-40.49	-50.57	-47.98	-51.78
$\Delta E + \Delta ZPE$	-32.55	-42.63	-38.56	-42.36
$\Delta E + \Delta ZPE$ -BSSE	-29.91	-34.98	-35.16	-32.34
N9H···OH···N3				
ΔE	-32.90	-46.50	-41.25	-48.53
$\Delta E + \Delta ZPE$	-25.60	-39.19	-32.51	-39.80
$\Delta E + \Delta ZPE$ -BSSE	-22.91	-31.76	-29.05	-30.47
N7···HOH···O=C6				
ΔE	-30.40	-38.17	-33.51	-38.82
$\Delta E + \Delta ZPE$	-22.84	-30.61	-24.89	-30.20
$\Delta E + \Delta ZPE$ -BSSE	-20.40	-23.40	-22.02	-22.39
Tautomer 3: Hydroxy-N9H Rotamer 1 (H9r1)				
N9H···OH···N3				
ΔE	-36.08	-49.21	-44.55	-51.15
$\Delta E + \Delta ZPE$	-28.47	-41.59	-35.64	-42.23
$\Delta E + \Delta ZPE$ -BSSE	-25.83	-34.19	-32.50	-32.83
C6OH···OH···N1				
ΔE	-33.47	-46.23	-45.22	-48.05
$\Delta E + \Delta ZPE$	-25.11	-37.87	-35.44	-38.28
$\Delta E + \Delta ZPE$ -BSSE	-21.55	-28.36	-33.04	-26.28
N7···HOH				
ΔE	-24.39	-32.49	-28.65	-32.84
$\Delta E + \Delta ZPE$	-18.52	-26.62	-22.02	-26.21
$\Delta E + \Delta ZPE$ -BSSE	-16.52	-21.12	-19.58	-19.44

of fact, the larger shifts -33 , -27 , and -19 cm⁻¹ for N7–H···O–H···O=C6 of O17, N1–H···O–H···O=C6 of O19, and

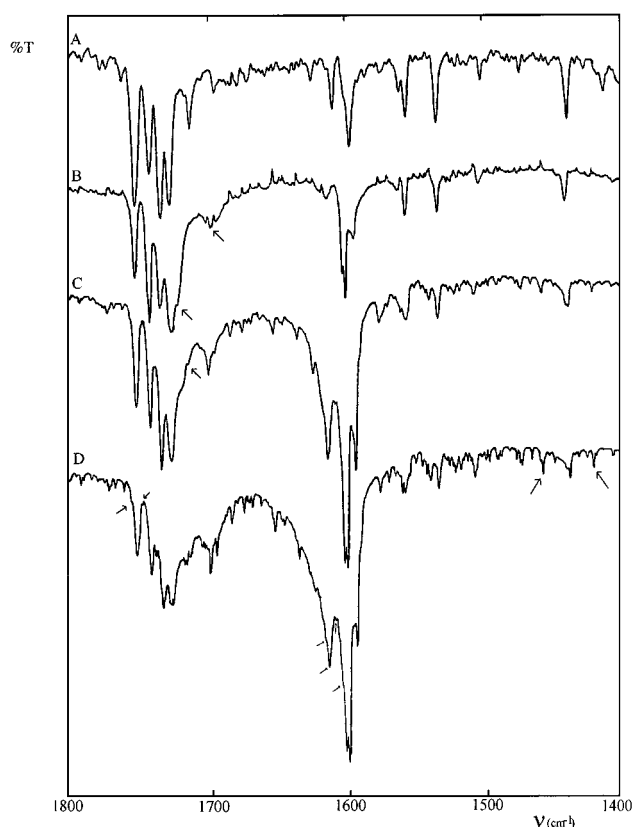


Figure 1. The $\nu_{C=O}$, δ_{H_2O} , and δ_{N-H} region of the FT-IR spectrum of hypoxanthine/Ar (A), hypoxanthine/H₂O/Ar (H₂O/Ar: 1/700) (B), hypoxanthine/H₂O/Ar (H₂O/Ar: 1/450) (C), and hypoxanthine/H₂O/Ar (H₂O/Ar: 1/300) (D).

N1–H···O–H···O=C6 of O17 correspond to $r_{C=O}$ increases of $+0.013$, $+0.012$, and $+0.014$ Å, respectively. The strongly different shift of $+4$ cm⁻¹ for N9–H···O–H···N3 of O19 is in accordance with a $r_{C=O}$ change of -0.001 Å only. It may be mentioned that a full quantitative comparison between $\Delta\nu_{C=O}$ and $\Delta r_{C=O}$ values for O17 and O19 complexes is not possible, since the $\nu_{C=O}$ modes have different potential energy distributions in the two hypoxanthine tautomers.⁴

Figure 1 also contains the δ_{N-H} spectral bands of the O17 and O19 hypoxanthine tautomers. The spectral analysis for the bonded δ_{N-H} modes in the four complexes considered is rather difficult because the intensities of these modes are much weaker than for the $\nu_{C=O}$ modes, the modes have only small δ_{N-H} PED

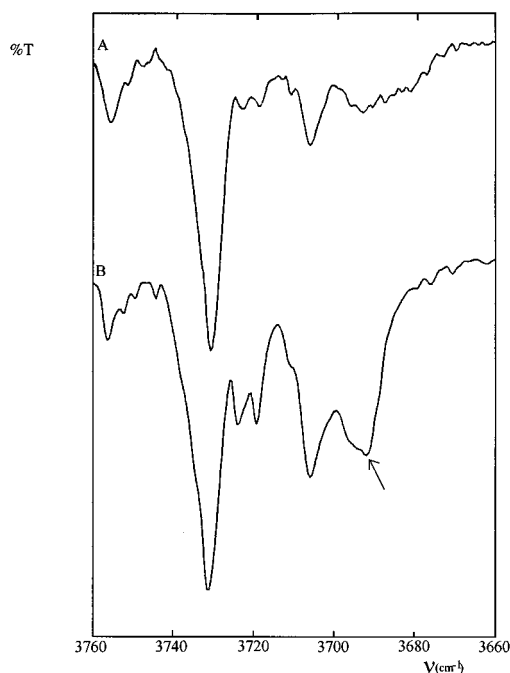


Figure 2. $\nu_{\text{O-H}}^{\text{f}}$ region of the spectra of water/Ar (A) and hypoxanthine/water/Ar ($\text{H}_2\text{O}/\text{Ar}$: 1/450) (B).

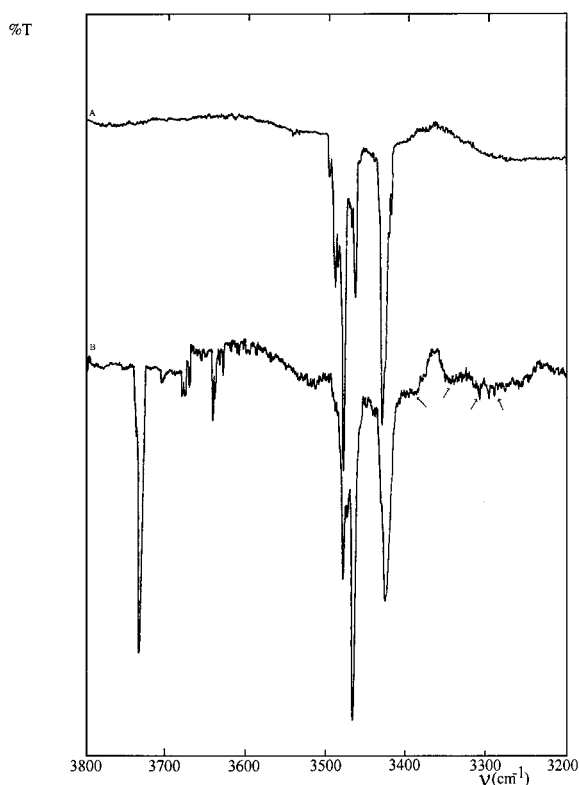


Figure 3. $\nu_{\text{N-H}}$ and $\nu_{\text{O-H}}^{\text{b}}$ regions of the FT-IR spectrum of hypoxanthine monomer (A) and hypoxanthine/ $\text{H}_2\text{O}/\text{Ar}$ ($\text{H}_2\text{O}/\text{Ar}$ = 1/300) (B).

contributions, and the predicted shifts for two different complexes of the same tautomer are sometimes very similar, e.g., +38 and +41 cm^{-1} for the two O17 complexes (Tables 4 and 5). Complex bands which can tentatively be assigned are the new bands at 1420 cm^{-1} (+32 cm^{-1}) for both $\text{N7-H}\cdots\text{O-H}\cdots\text{O}=\text{C6}$ and $\text{N1-H}\cdots\text{O-H}\cdots\text{O}=\text{C6}$ of O17 and 1457 cm^{-1} (+33 cm^{-1}) for $\text{N1-H}\cdots\text{O-H}\cdots\text{O}=\text{C6}$ of O19.

The $\delta(\text{H}_2\text{O})$ region can hardly be used for spectral analysis, because overlap with hypoxanthine modes, e.g., $\nu(\text{C2N3})$,⁴

occurs, coupling with an internal O17 hypoxanthine mode ν -(C2N3) is observed for $\text{N7-H}\cdots\text{O-H}\cdots\text{O}=\text{C6}$ of O17 (Table 4) and the predicted shifts for the other three complexes are very similar (+12, +17, +15 cm^{-1}). The assignments listed in Tables 4–7 are therefore extremely tentative.

$\nu_{\text{O-H}}^{\text{f}}$ Region (Figure 2). The four complexes identified in the $\nu_{\text{C=O}}$ region appear to be all characterized by similar predicted shifts of the non-H-bonded water stretching mode $\nu_{\text{O-H}}^{\text{f}}$, i.e., -35 ($\text{N7-H}\cdots\text{O-H}\cdots\text{O}=\text{C6}$ of O17), -37 ($\text{N1-H}\cdots\text{O-H}\cdots\text{O}=\text{C6}$ of O19), -36 ($\text{N1-H}\cdots\text{O-H}\cdots\text{O}=\text{C6}$ of O17), and -33 ($\text{N9-H}\cdots\text{O-H}\cdots\text{N3}$ of O19) cm^{-1} (Tables 4–7). Figure 2 illustrates the $\nu_{\text{O-H}}^{\text{f}}$ region of the spectra of water/Ar (A) and hypoxanthine/water/Ar (B). New and broader bands are observed in the hypoxanthine/water spectrum (B) in the region of 3690 cm^{-1} . They overlap more or less with some bands of dimer, trimer, or polymer associates (H_2O)_n (A),³⁴ although they are somewhat larger. In conclusion, this spectral region is suitable to identify H-bonding of water with hypoxanthine qualitatively, but it does not allow discrimination among the four different complexes.

$\nu_{\text{O-H}}^{\text{b}}$ and $\nu_{\text{N-H}}$ Region (Figure 3). Figure 3 illustrates the spectral region 3800–3200 cm^{-1} which contains the $\nu_{\text{N-H}}$ modes of the complexed hypoxanthine tautomers as well as the important $\nu_{\text{O-H}}^{\text{b}}$ mode of H-bonded water. Because of the presence of many disturbing absorptions due to self-associated water (dimers, trimers, ...) in spectra of matrix samples with high water content, the analysis of this spectral region has been based on samples with low water content only.

A number of new, broad bands are observed on addition of water to hypoxanthine/Ar, i.e., at 3392, 3346, and at 3260–3220 cm^{-1} , the latter band being a very broad structure due to overlapping bands. Also, some broader absorptions appear superimposed on the free ν_{NH} modes of hypoxanthine (3480–3420 cm^{-1}). The origin of these bands is due to either the bonded $\nu_{\text{O-H}}^{\text{b}}$ or the $\nu_{\text{N-H}}$ modes in the different complexes, and the theoretical predictions (Tables 4–7) may serve as a guide for their assignment.

Frequency shifts of -294, -235, -255, and -184 cm^{-1} are predicted for the $\nu_{\text{O-H}}^{\text{b}}$ mode of water bonded in the closed complexes $\text{N7H}\cdots\text{O-H}\cdots\text{O}=\text{C6}$ (O17), $\text{N1-H}\cdots\text{O-H}\cdots\text{O}=\text{C6}$ (O17), $\text{N1-H}\cdots\text{O-H}\cdots\text{O}=\text{C6}$ (O19), and $\text{N9-H}\cdots\text{O-H}\cdots\text{N3}$ (O19), respectively. This allows the bands observed at 3346 and 3392 cm^{-1} to be assigned to the $\nu_{\text{O-H}}^{\text{b}}$ mode in the $\text{N7-H}\cdots\text{O-H}\cdots\text{O}=\text{C6}$ (O17) and the $\text{N1-H}\cdots\text{O-H}\cdots\text{O}=\text{C6}$ (O19) complexes, respectively, with experimental shifts of -327 and -281 cm^{-1} . It must be mentioned that the experimental frequencies have been corrected for the reduced coupling between the two O–H vibrations in bonded water by the procedure described earlier.⁸ However, in the case of a closed H-bonded complex this correction is relatively small due to the larger difference between the free O–H bond and the doubly bonded O–H group. Based on the theoretical predictions, the corresponding $\nu_{\text{O-H}}^{\text{b}}$ modes of the two other complexes, $\text{N1-H}\cdots\text{O-H}\cdots\text{O}=\text{C6}$ (O17) and $\text{N9-H}\cdots\text{O-H}\cdots\text{O}=\text{C6}$ (O19) might be assigned to the broader bands above the free $\nu_{\text{N-H}}$ structure at 3450 and 3470 cm^{-1} .

Although the above assignments are somewhat tentative, two further arguments give additional support. First of all, the optimal scaling factors $\nu_{\text{exp}}/\nu_{\text{calc}}$ are all around 0.96 for the four different complexes (Tables 4–7). We have formerly demonstrated from a correlation between this optimal scaling factor and the frequency shift $\Delta\nu_{\text{O-H}}^{\text{b}}$ that optimal scaling factors of 0.85–0.84 correspond with frequency shifts in the range 200–300 cm^{-1} when RHF/6-31++G** predictions are used.³⁷ Since

TABLE 4: Experimental (Ar Matrix) and Calculated (DFT/B3LYP/6-31++G) IR Spectral Data for the Closed Complex N7–H···O–H···O=C6 of O17-Hypoxanthine with Water**

exptl ν , cm^{-1}	$\Delta\nu$, ^a cm^{-1}	calcd (DFT/B3LYP)			optimal scaling factor ^c	PED ^d
		ν , cm^{-1} , nonscaled/scaled variable scaling factor ^b	I , $\text{km}\cdot$ mol^{-1}	$\Delta\nu$, ^a cm^{-1}		
Water Modes						
3706/3701/3696/3692	-28 → -42	3894/3700	95	-35	0.950	$\nu^f(\text{OH})(96)$
3346 → 3359 ^e	-292 → -327 ^e	3499/3324	789	-294	0.956	$\nu^b(\text{OH})(93)$
1613?	+22	{ 1647/1606 1632/1591	{ 123 148	{ +46 +31	0.979	$\delta(\text{H}_2\text{O})(63) + \nu(\text{C}_2\text{N}_3)(21)$
680		737/722	181		0.923	$\delta(\text{H}_2\text{O})(45) + \nu(\text{C}_2\text{N}_3)(28)$ $\tau^1(\text{OHH})(55) + \tau^2(\text{OHH})(32)^f$
Hypoxanthine (O17) Modes						
3220	-259	3378/3209	412	-263	0.953	$\nu(\text{N7H})(94)$
±1700	-34/-28	1740/1696	758	-33	0.977	$\nu(\text{C6O})(52) + \nu(\text{C5C6})(20)$
1570	+37	1561/1522	30	+4 (? ?)	1.006	$\delta(\text{N7H})(28) + \nu(\text{C8N9})(11) + \nu(\text{C2N3})(11) + \nu(\text{C5N7})(11)$
1420	+32	1477/1440	86	+38	0.961	$\delta(\text{N7H})(26) + \nu(\text{N7C8})(22) + \delta(\text{C8H})(19)$
810	+285	831/815	125	+298	0.975	$\gamma(\text{N7H})(89)$
too weak		727/712	21	-4		$\gamma(\text{C6O})(63) + \gamma(\text{N1H})(28)$

^a Shift with respect to experimental or calculated (scaled) monomer frequencies. ^b Variable scaling factor: 0.950 for $\nu(\text{XH})$, 0.98 for γ and τ , and 0.975 for all other modes. ^c Optimal scaling factor = $\nu_{\text{exp}}/\nu_{\text{calc}}$. ^d ν = stretching, δ = bending, τ = torsion, γ = out of plane motion, f = free, non-hydrogen-bonded, b = hydrogen bonded. ^e $\nu^b(\text{OH})$ is corrected for reduced coupling in bonded water. ^f One of the six new intermolecular modes.

TABLE 5: Experimental (Ar Matrix) and Calculated (DFT/B3LYP/6-31++G) IR Spectral Data for the Closed Complex N1–H···O–H···O=C6 of O17 Hypoxanthine with Water**

exptl ν , cm^{-1}	$\Delta\nu$, ^a cm^{-1}	calcd (DFT/B3LYP)			optimal scaling factor ^c	PED ^d
		ν , cm^{-1} , nonscaled/scaled variable scaling factor ^b	I , $\text{km}\cdot$ mol^{-1}	$\Delta\nu$, ^a cm^{-1}		
Water Modes						
3706/3701/3696/3692	-28 → -42	3894/3699	99	-36	0.950	$\nu^f(\text{OH})(95)$
3440 → 3453 ^e	-198 → -233 ^e	3561/3383	576	-235	0.966	$\nu^b(\text{OH})(93)$
1605	+14	1612/1572	277	+12	0.996	$\delta(\text{H}_2\text{O})(97)$
630 (br)		677/663	252		0.930	$\tau^1(\text{OHH})(57) + \tau^2(\text{OHH})(40)^f$
Hypoxanthine (O17) Modes						
3260	-211	3401/3231	372	-192	0.958	$\nu(\text{N1H})(97)$
1715	-19/-13	1754/1710	752	-19	0.978	$\nu(\text{C6O})(47) + \nu(\text{C5C6})(18) + \delta(\text{N1H})(13)$
1420	+32	1480/1443	27	+41	0.959	$\delta(\text{N1H})(39) + \nu(\text{C6O})(15) + \nu(\text{C8N9})(10)$
840	+181	855/837	116	+179	0.982	$\gamma(\text{N1H})(94)$
too weak		715/701	0.2	-15		$\gamma(\text{C6O})(49) + \tau\text{R}(27) + \tau\text{R}(13)$

^a Shift with respect to experimental or calculated (scaled) monomer frequencies. ^b Variable scaling factor: 0.950 for $\nu(\text{XH})$, 0.98 for γ and τ and 0.975 for all other modes. ^c Optimal scaling factor = $\nu_{\text{exp}}/\nu_{\text{calc}}$. ^d ν = stretching, δ = bending, τ = torsion, γ = out of plane motion, f = free, non-hydrogen bonded, b = hydrogen bonded. ^e $\nu^b(\text{OH})$ is corrected for reduced coupling in bonded water. ^f One of the six new intermolecular modes.

scaling factors in RHF and DFT differ by $(0.90 \times 0.95) = 0.85$, the obtained optimal scaling factors and therefore the $\nu_{\text{O-H}}^b$ assignments are in line with earlier results for B···HO H-bonded systems. On the other hand, an additional experiment with D₂O was performed and the result is illustrated in Figure 4. In this spectrum of a hypoxanthine/D₂O/Ar sample with relatively high water content, all the typical monomer, dimer, trimer, and even multimer D₂O absorptions assigned by Bentwood et al.³⁴ appear. However, additional bands not assignable to the monomer or to any self-associated species appear at 2620 (weak), 2590, 2555, and 2520 cm^{-1} . By comparison with the earlier assigned $\nu_{\text{O-H}}^b$ modes at 3470, 3440, 3392, and 3346 cm^{-1} , isotopic ratios $\nu_{\text{O-H}}^b/\nu_{\text{O-D}}^b$ of 1.324, 1.328, 1.328, and 1.328 are obtained, which are quite acceptable values for H-bonded systems of this strength.⁶

The bonded N–H stretching mode is predicted to shift -263, -192, -201, and -138 cm^{-1} in the N7–H···O–H···O=C6 (O17), N1–H···O–H···O=C6 (O17), N1–H···O–H···O=C6 (O19), and N9–H···O–H···N3 (O19) complexes, respectively. The broad complex structure observed at 3260–3220 cm^{-1} , with some indication of contributing absorptions at 3260, 3240, and

3220 cm^{-1} , is most probably the result of the close-lying $\nu_{\text{N-H}}$ bands of the three most stable complexes (see Tables 4–6). It must be mentioned that the problem of overlapping complex bands is purely accidental in this case, since relatively large differences in shift, e.g., -263 compared to -192, are canceled by the frequency differences of the free N7–H and N1–H stretch in O17 hypoxanthine. The new band at 3325 cm^{-1} can be tentatively assigned to the same mode in the least stable complex N9–H···O–H···O=C6 (O19). All the experimental shifts agree well with the predicted shifts, while the optimal scaling factors of 0.96–0.95 are again in accordance with earlier results for N–H···O–H complexes.

It may be concluded that the $\nu_{\text{N-H}}$ region cannot be used for detailed spectral analysis of the H-bonding by accidental overlap, while the $\nu_{\text{O-H}}^b$ region is informative although care must be taken.

H-Bonded $\tau(\cdots\text{OHH}\cdots)$ Mode. H-bonding of water by a base yields six new intermolecular vibrations, one of these being located in the mid-IR range of the spectrum, usually as a broad band between 700 and 500 cm^{-1} .³⁸ Tables 4–7 also list the frequency predictions for this intermolecular mode. Three broad

TABLE 6: Experimental (Ar Matrix) and Calculated (DFT/B3LYP/6-31++G) IR Spectral Data for the Closed Complex N1-H...O-H...O=C6 of O19 Hypoxanthine with Water**

exptl ν, cm^{-1}	$\Delta\nu,^a$ cm^{-1}	calcd (DFT/B3LYP)			$\Delta\nu,^a$ cm^{-1}	optimal scaling factor ^c	PED ^d
		$\nu,^b \text{cm}^{-1}$, nonscaled/scaled variable scaling factor	$I, \text{km}\cdot\text{mol}^{-1}$				
Water Modes							
3706/3701/36 96/3692	-28 → -42	3893/3698	95	-37	0.950	$\nu^f(\text{OH})(95)$	
3392 → 3405 ^e	-246 → -281 ^e	3540/3363	650	-255	0.958	$\nu^b(\text{OH})(92)$	
1617	+26	1617/1577	199	+17	1	$\delta(\text{H}_2\text{O})(88)$	
630 (br)		691/677	261		0.912	$\tau^1(\text{OHH})(54) + \tau^2(\text{OHH})(36)^f$	
Hypoxanthine (O19) Modes							
3240	-188	3388/3219	369	-201	0.956	$\nu(\text{N1H})(97)$	
1722	-31/-20	1771/1726	717	-27	0.972	$\nu(\text{C6O})(57) + \nu(\text{C5C6})(14) + \delta(\text{N1H})(12)$	
1457	+33	1539/1500	30	+54	0.947	$\delta(\text{N1H})(25) + \nu(\text{C6O})(14) + \nu(\text{N7C8})(13) + \nu(\text{C4C5})(11)$	
840	+139	866/849	125	+136	0.970	$\gamma(\text{N1H})(90)$	
too weak	695/681	5	-78	$\gamma(\text{C6O})(36) + \tau\text{r1}(26) + \tau\text{rR}(15)$			

^a Shift with respect to experimental or calculated (scaled) monomer frequencies. ^b Variable scaling factor: 0.950 for $\nu(\text{XH})$, 0.98 for γ and τ , and 0.975 for all other modes. ^c Optimal scaling factor = $\nu_{\text{exp}}/\nu_{\text{calc}}$. ^d ν = stretching, δ = bending, τ = torsion, γ = out of plane motion, f = free, non-hydrogen-bonded, b = hydrogen bonded. ^e $\nu^b(\text{OH})$ is corrected for reduced coupling in bonded water. ^f One of the six new intermolecular modes.

TABLE 7: Experimental (Ar Matrix) and Calculated (DFT/B3LYP/6-31++G) IR Spectral Data for the Closed Complex N9-H...O-H...N3 of O19 Hypoxanthine with Water**

exptl ν, cm^{-1}	$\Delta\nu,^a$ cm^{-1}	calcd (DFT/B3LYP)			$\Delta\nu,^a$ cm^{-1}	optimal scaling factor ^c	PED ^d
		ν, cm^{-1} , nonscaled/scaled variable scaling factor ^b	$I, \text{km}\cdot\text{mol}^{-1}$				
Water Modes							
3706/3701/36 96/3692	-28 → -42	3897/3702	112	-33	0.949	$\nu^f(\text{OH})(94)$	
3470 → 3483 ^e	-168 → -203 ^e	3614/3434	458	-184	0.960	$\nu^b(\text{OH})(93)$	
1609	+18	1615/1575	87	+15	0.996	$\delta(\text{H}_2\text{O})(83)$	
570 (weak)		625/612	140		0.912	$\tau^1(\text{OHH})(49) + \tau^2(\text{OHH})(34)^f$	
Hypoxanthine (O19) Modes							
3325	-140	3509/3334	267	-138	0.948	$\nu(\text{N9H})(97)$	
1757/1749	+4/+15	1802/1757	753		0.975	$\nu(\text{C6O})(73) + \nu(\text{C5C6})(13)$	
	-4/+7			+4	0.971		
too weak		1420/1385	55	+13		$\delta(\text{N9H})(26) + \nu(\text{C4C5})(14) + \nu(\text{C8N9})(14) + \delta(\text{N1H})(11)$	
694?	+184	757/742	77	+226	0.917	$\gamma(\text{N9H})(77)$	

^a Shift with respect to experimental or calculated (scaled) monomer frequencies. ^b Variable scaling factor: 0.950 for $\nu(\text{XH})$, 0.98 for γ and τ , and 0.975 for all other modes. ^c Optimal scaling factor = $\nu_{\text{exp}}/\nu_{\text{calc}}$. ^d ν = stretching, δ = bending, τ = torsion, γ = out of plane motion, f = free, non-hydrogen-bonded, b = hydrogen bonded. ^e $\nu^b(\text{OH})$ is corrected for reduced coupling in bonded water. ^f One of the six new intermolecular modes.

bands are observed in the experimental complex spectra at 680, 630, and 570 cm^{-1} . Comparison with the frequency predictions allows assignment of the band at 680 cm^{-1} to the H-bond torsion in the complex N7-H...O-H...O=C6 (O17), the band at 630 cm^{-1} to that mode in the complexes N1-H...O-H...O=C6 (O17) and N1-H...O-H...O=C6 (O19), and the band at 570 cm^{-1} to the torsion in the complex N9-H...O-H...O=C6 (O19). The smaller optimal scaling factors (0.93–0.91) obtained for this mode reflect the larger anharmonicity of this intermolecular torsion.

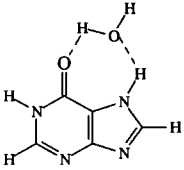
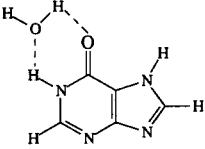
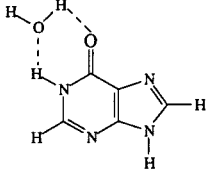
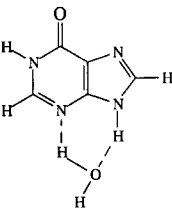
Correlations. From the above analysis some interesting correlations between theoretical and experimental H-bond parameters can be derived.

Figure 5 shows the correlation between the experimental and theoretical frequency shift of the $\nu_{\text{N-H}}$ vibration and the theoretical H-bond angle $\alpha(\text{N-H}\cdots\text{O})$ in complexes of the types N-H...O-H...X and N-H...O=C-N-H...X. From this correlation it is obvious that there is a clear relationship between the strength of the H-bond ($\Delta\nu_{\text{N-H}}$) and the linearity of the H-bond. The closer the H-bond angle approaches linearity, the

larger is the frequency shift and thus the charge transfer in the complex. In other words, an increasing linearity of the hydrogen bonds increases the cooperativity between the two H-bonds in the closed complexes. The correlation shown in Figure 5 is based on four different complexes of 2-pyridone and hypoxanthine. The point at largest $\Delta\nu_{\text{N-H}}$ is for the 2-pyridone dimer, which is an almost linear and very strong complex. This correlation shows also the overestimation of the frequency shift by the B3-LYP functional for complexes with a bond angle smaller than 170° (moderately strong H-bond), as was already found earlier.³⁵

A second correlation (Figure 6) is that between the experimental, relative frequency shift $\Delta\nu(\text{N-H}\cdots)/\nu^0(\text{N-H})$ and the calculated interaction energy at the DFT level. From this correlation a clear difference is observed between the open N-H...OH₍₂₎ complexes and the closed N-H...O-H...X complexes. As expected, the interaction energy for the closed (N-H...O-H...N) complexes is much higher than for open (N-H...OH₍₂₎) complexes at a constant frequency shift. This

TABLE 8: Selected Structural Properties (Distances (Å) and Angles (deg)) for Different Complexes of Hypoxanthine with Water

								
	N7-H...O-H...O=C6		N1-H...O-H...O=C6		N1-H...O-H...O=C6		N9-H...O-H...N3	
	DFT	RHF	DFT	RHF	DFT	RHF	DFT	RHF
...O-H...								
R(O...O)	2.765	2.865	2.759	2.859	2.748	2.848	2.872 (O...N)	3.017 (O...N)
r(O-H) ^{bonded}	0.984	0.953	0.981	0.951	0.982	0.952	0.978	0.949
r(O-H) ^{free}	0.964	0.942	0.964	0.942	0.964	0.942	0.964	0.943
α(O-H...O)	158.15	152.71	145.88	139.94	146.76	140.53	142.42 (O-H...N)	137.12 (O-H...N)
-N-H monomer	N7-H		N1-H		N1-H		N9-H	
	1.010	0.994	1.014	0.997	1.014	0.997	1.010	0.994
-N-H...								
R(N...O)	2.792	2.903	2.829	2.939	2.830	2.943	2.829	2.920
r(N-H)	1.026	1.002	1.025	1.003	1.026	1.003	1.019	0.999
α(N-H...O)	146.12	146.06	142.97	144.04	144.45	145.53	133.68	136.04
-C=O monomer	1.229	1.203	1.229	1.203	1.221	1.195	1.221	1.195
-C=O...								
r(C=O)	1.242	1.213	1.243	1.213	1.233	1.204	1.220	1.195
r(O...H)	1.827	1.985	1.892	2.064	1.873	2.048	2.035 (N...H)	2.251 (N...H)
α(C=O...H)	115.29	118.95	109.21	111.89	110.83	113.75		

illustrates that the cooperativity effect, due to the formation of a second H-bond, is more reflected by the interaction energy than by the frequency shift. The additional frequency shift caused by the H-bond cooperativity of the bonded N-H group is thus rather limited for this type of closed complex. On the other hand, for the N-H...O-H...O=C complexes the extra frequency shift of the bonded N-H group is more pronounced, which is probably due to the larger basicity of the C=O group compared to the N atom. Both types of hypoxanthine complexes

(N-H...O-H...N and N-H...O-H...O=C), studied in this work, are included in this correlation.

At last, Figure 7 illustrates the correlation between the optimal scaling factor ($\nu_{\text{exp}}/\nu_{\text{calc}}$) for the bonded water vibration $\nu_{\text{OH}}^{\text{b}}$ (DFT level) and the experimental proton affinity ($\text{kJ}\cdot\text{mol}^{-1}$). Also from this correlation the difference between open and closed complexes is clear. The smaller value of the optimal scaling factor in closed complexes results from the higher anharmonicity of the H-bond interaction. It was noticed before

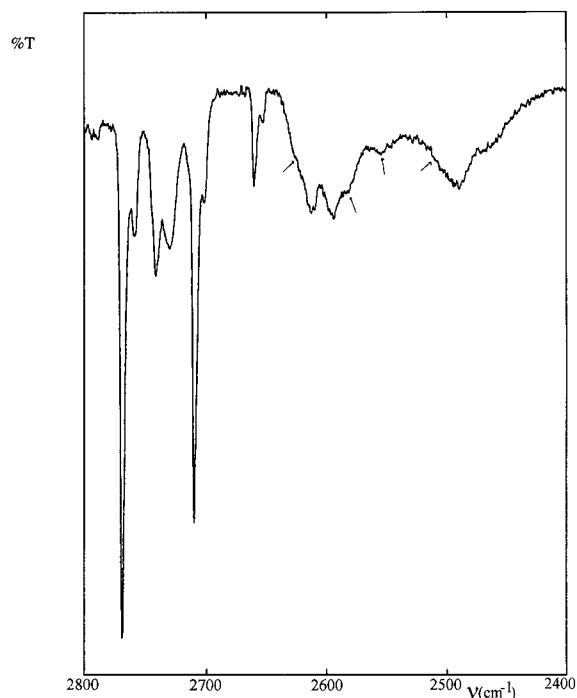


Figure 4. The 2800–2400 cm^{-1} region of the FT-IR spectrum of hypoxanthine/ $\text{D}_2\text{O}/\text{Ar}$ ($\text{D}_2\text{O}/\text{Ar}$: 1/200).

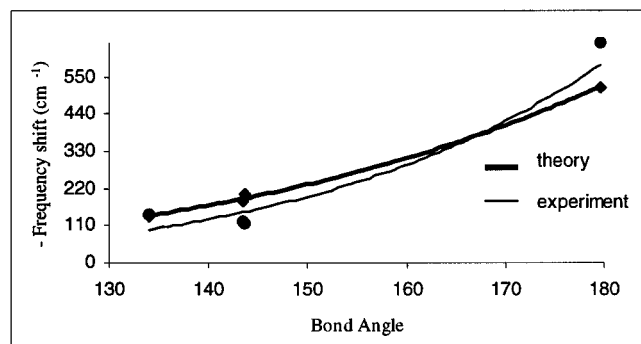


Figure 5. Correlation between the frequency shift $\Delta\nu_{\text{N-H}}$ (cm^{-1}) and the H-bond angle $\alpha(\text{N-H}\cdots\text{O})$ (deg) in complexes of the type $\text{N-H}\cdots\text{O-H}\cdots\text{X}$ and $\text{N-H}\cdots\text{O}=\text{C-N-H}\cdots\text{X}$ for hypoxanthine and 2-pyridone.

that the optimal scaling factor for the $\nu_{\text{OH}}^{\text{b}}$ mode decreases with increase of the H-bond strength.³⁶ This correlation can be used for the estimation of the proton affinity for molecules in open complexes. The proton affinity is an important parameter for the determination of the strength of H-bonds.

Conclusions

The combined matrix-isolation FT-IR and theoretical methodology applied to the H-bonding of hypoxanthine tautomers with water leads to the following conclusions:

1. All the theoretical methods predict that the H-bonded complex $\text{N7-H}\cdots\text{O-H}\cdots\text{O}=\text{C6}$ of the O17 hypoxanthine tautomer is the most stable H-bonded system between hypoxanthine and water. No tautomeric shift is predicted for the interaction of hypoxanthine with one water molecule. Less stable complexes are the $\text{N1-H}\cdots\text{O-H}\cdots\text{O}=\text{C6}$ complex of the O17 tautomer and two closed complexes of the O19 form, i.e., $\text{N1-H}\cdots\text{O-H}\cdots\text{O}=\text{C6}$ and $\text{N9-H}\cdots\text{O-H}\cdots\text{N3}$.

2. These four complexes are all identified in the experimental matrix FT-IR spectrum. The $\text{N7-H}\cdots\text{O-H}\cdots\text{O}=\text{C6}$ is experimentally the most abundant form.

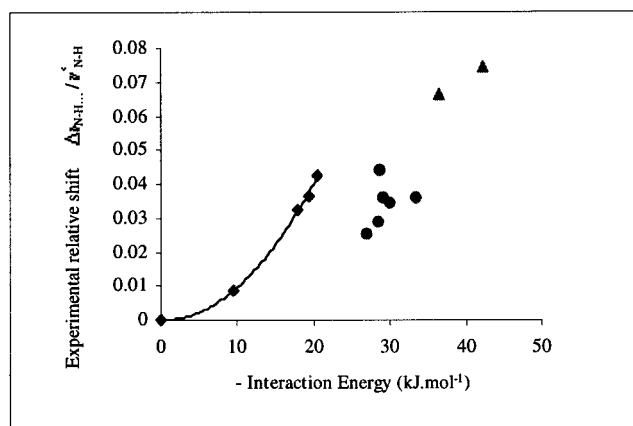


Figure 6. Correlation between the experimental, relative frequency shift $\Delta\nu(\text{N-H}\cdots)/\nu^{\circ}(\text{N-H})$ and the DFT calculated interaction energy for complexes of the type $\text{N-H}\cdots\text{O-H}(\cdots\text{X})$ \blacklozenge : $\text{N-H}\cdots\text{O-H}$ open complexes (imidazole, benzimidazole, 4- NH_2 -benzimidazole) \bullet : $\text{N-H}\cdots\text{O-H}\cdots\text{N}$ closed complexes (adenine, 4(7)- NH_2 -benzimidazole and hypoxanthine) \blacktriangle : $\text{N-H}\cdots\text{O-H}\cdots\text{O}=\text{C}$ closed complexes (hypoxanthine, 2-OH-pyridine).

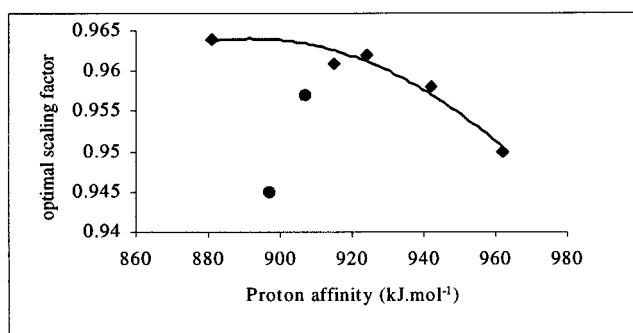


Figure 7. Correlation between the optimal scaling factor ($\nu_{\text{exp}}/\nu_{\text{calc}}$) and the proton affinity ($\text{kJ}\cdot\text{mol}^{-1}$) for complexes of the type $\text{N}\cdots\text{H-O}(\cdots\text{H-X})$ \blacklozenge : $\text{N}\cdots\text{H-O}$ open complexes (pyrimidine, 3-OH-pyridine, pyridine, 4-OH-pyridine and 4- NH_2 -pyridine)³⁶ \bullet : $\text{N}\cdots\text{H-O}\cdots\text{H-X}$ closed complexes (2-OH-pyridine and hypoxanthine).

3. Among the four stable H-bonded complexes, the closed complexes with two H-bonds are more stable than the open complexes and these are characterized by a sensitively larger H-bond interaction energy. This is due to the cooperativity effect between the two H-bonds in a closed complex. The $\text{N7}\cdots\text{H-O-H}\cdots\text{O}=\text{C6}$ complex of the O19 tautomer is also a closed complex, but it is much weaker due to the anticooperativity effect.

4. Analysis of the vibrational modes directly involved in the H-bond interaction allows the identification of the different complexes in the experimental low-temperature matrix IR spectrum. The $\nu_{\text{C}=\text{O}}$ region is the most suitable spectral region for identification of the three most stable complexes, because in this region all the characteristic bands are clearly separated. The $\nu_{\text{OH}}^{\text{b}}$ region is also informative, but additional experiments with D_2O are preferable.

The $\nu_{\text{O-H}}^{\text{f}}$ and $\nu_{\text{N-H}}$ modes cannot be used to discriminate among the different complexes.

The agreement between experimental and calculated (DFT/B3LYP) frequencies of the H-bonded complexes is satisfying, especially when variable scaling factors are used.

The experimental and theoretical data obtained in these and previous studies allow interesting correlations to be established between some experimental and calculated parameters such as frequency shifts, structural parameters, proton affinities, and optimal scaling factors. From these correlations it is clear that

the H-bond cooperativity in closed complexes depends on the linearity of the H-bonds. The latter property is reflected by the intermolecular H-bond distance and by the frequency shift of the stretching mode $\Delta\nu_{\text{NH}}$ directly involved in the N—H \cdots O H-bond.

Acknowledgment. R. Ramaekers acknowledges financial support from the Belgian IWT.

References and Notes

- (1) Saenger W. *Principles of Nucleic Acid Structure*; Springer: New York, 1984.
- (2) Stryer L. *Biochemistry*; W. H. Freeman and Company: New York, 1988.
- (3) Friedberg E. C.; Walker G. C.; Siede W. *DNA Repair and Mutagenesis*; ASM Press: Washington, DC, 1995.
- (4) Ramaekers R.; Maes G.; Adamowicz L.; Dkhissi A. *J. Mol. Struct.* **2001**, *560*, 205.
- (5) Buyl F.; J. Smets; G. Maes; L. Adamowicz, *J. Phys. Chem.* **1995**, *99*, 14967.
- (6) Smets J.; Destexhe A.; Adamowicz L.; Maes G. *J. Phys. Chem. A* **1998**, *102*, 8157.
- (7) Smets J.; Adamowicz L.; Maes G. *J. Phys. Chem.* **1996**, *100*, 6434.
- (8) Houben L., Ph.D. Thesis, KULeuven, 2000.
- (9) Maes G. *Bull. Soc. Chim. Belg.* **1981**, *90*, 1093.
- (10) Graindourze M.; Smets J.; Zeegers-Huyskens Th.; Maes G. *J. Mol. Struct.* **1990**, *222*, 345.
- (11) Becke A. D. *J. Chem. Phys.* **1993**, *98*, 5648.
- (12) Lee C.; Yang W.; Parr R. G. *Phys. Rev. B* **1988**, *37*, 785.
- (13) Van Bael M. K.; Schoone K.; Houben L.; Smets J.; McCarthy W.; Adamowicz L.; Nowak M. J.; Maes G. *J. Phys. Chem. A* **1997**, *101*, 2397.
- (14) Schoone K.; Smets J.; Houben L.; Van Bael M. K.; Adamowicz L.; Maes G. *J. Phys. Chem. A* **1998**, *102*, 4863.
- (15) Hobza P.; Spöner J.; Reschel T. *J. Comput. Chem.* **1995**, *1611*, 1315.
- (16) Dkhissi A.; Adamowicz L.; Maes G. *J. Phys. Chem. A* **2000**, *104*, 2112.
- (17) Dkhissi A.; Houben L.; Smets J.; Adamowicz L.; Maes G. *J. Phys. Chem. A* **2000**, *104*, 9785.
- (18) Maes G.; Smets J.; Adamowicz L.; McCarthy W.; Van Bael M. K.; Houben L.; Schoone K. *J. Mol. Struct.* **1997**, *410–411*, 315.
- (19) Smets J.; McCarthy W.; Maes G.; Adamowicz L. *J. Mol. Struct.* **1999**, *476*, 27.
- (20) Boys S. F.; Bernardi F. *Mol. Phys.* **1970**, *19*, 553.
- (21) Gaussian94; Revision E.2. Frisch, M. J.; Trucks, G. W.; Schlegel, H. B.; Gill, P. M. W.; Johnson, B. G.; Robb, M. A.; Cheeseman, J. R.; Keith, T.; Petersson, G. A.; Montgomery, J. A.; Raghavachari, K.; Al-Laham, M. A.; Zakrzewski, V. G.; Ortiz, J. V.; Foresman, J. B.; Cioslowski J.; Stefanov B. B.; Nanayakkara, A.; Challacombe M.; Peng, C. Y.; Ayala, P. Y.; Chen, W.; Wong, M. W.; Andres, J. L.; Replogle, E. S.; Gomperts, R.; Martin, R. L.; Fox, D. J.; Binkley, J. S.; Defrees, D. J.; Baker, J.; Stewart, J. P.; Head-Gordon, M.; Gonzales, C.; Pople, J. A., Gaussian Inc.: Pittsburgh, PA, 1995.
- (22) Gaussian98, Revision A. 5. Frisch, M. J.; Trucks, G. W.; Schlegel, H. B.; Scuseria G. E.; Robb, M. A.; Cheeseman, J. R.; Zakrzewski, V. G.; Montgomery, J. A.; Stratmann, R. E.; Burant, J. R.; Dapprich S.; Millam, J. M.; Daniels, A. D.; Kudin, K. N.; Strain, M. C.; Farkas, O.; Tomasi, J.; Barone, V.; Cossi, M.; Cammi, R.; Mennucci, B.; Pomelli, C.; Adamo, C.; Clifford, S.; Ochterski, J.; Petersson G. A.; Ayala P. Y., Cui Q.; Morokuma K.; Malick, D. K.; Rabuck, A. D.; Raghavachari, K.; Foresman, J. B.; Cioslowski, J.; Ortiz, J. V.; Stefanov, B. B.; Liu, G.; Liashenko, A.; Piskorz, P.; Komaromi, I.; Gomperts, R.; Martin, R. L.; Fox, D. J.; Keith, T.; Al-Laham, M. A.; Peng, C. Y.; Nanayakkara, A.; Gonzalez, C.; Challacombe, M.; Gill, P. M. W.; Johnson, B. G.; Chen, W.; Wong, M. W.; Andres, J. L.; Head-Gordon, M.; Replogle, E. S.; Pople J. A. Gaussian, Inc., Pittsburgh, PA, 1998.
- (23) Florian J.; Johnson B. G. *J. Phys. Chem.* **1994**, *98*, 3681.
- (24) Rauhut G.; Pulay P. *J. Phys. Chem.* **1995**, *99*, 3093.
- (25) Florian J.; Leszczynski J. *J. Phys. Chem.* **1996**, *100*, 5578.
- (26) Dkhissi A.; Houben L.; Smets J.; Adamowicz L.; Maes G. *J. Mol. Struct.* **1999**, *484*, 215.
- (27) Costas M. E.; Acevedo-Chàvez R. *J. Phys. Chem. A* **1997**, *101*, 8309.
- (28) Barone V.; Adamo C. *J. Phys. Chem.* **1995**, *99*, 15062.
- (29) Sheina G. G.; Stepanian S. G.; Radchenko E. D.; Blagoi Y. P. *J. Mol. Struct.* **1987**, *158*, 275.
- (30) Maes G.; Smets J. *J. Phys. Chem.* **1993**, *97*, 1818. Kleeberg H.; Klein D.; Luck W. A. P. *J. Phys. Chem.* **1987**, *91*, 3200. Huyskens P. L. *J. Am. Chem. Soc.* **1977**, *99*, 2578.
- (31) Dkhissi A.; Houben L.; Ramaekers R.; Adamowicz L.; Maes G. *J. Phys. Chem. A* **1999**, *103*, 50, 11020.
- (32) Dkhissi A.; Adamowicz L.; Maes G. *J. Phys. Chem. A* **2000**, *104*, 5625.
- (33) Shukla, M. K.; Leszczynski, J. *J. Phys. Chem. A* **2000**, *104*, 3021.
- (34) Bentwood R. M.; Barnes A. J.; Orville-Thomas W. J. *J. Mol. Spectrosc.* **1980**, *84*, 391.
- (35) Dkhissi A.; Alikhani M. E.; Bouteiller Y. *J. Mol. Struct.* **1997**, *416*, 1.
- (36) Smets, J. Ph.D. Thesis, KULeuven, 1993.
- (37) Schoone, K. MS Thesis, KULeuven, 1995.
- (38) Person W. B.; Del Bene J. E.; Szajda W.; Szczepaniak K.; Szczepniak M. *J. Phys. Chem.* **1991**, *95*, 2770.